although the potency of CO is far less than that of NO in vitro.[12–14] Such interactions among the gas-producing or receptor systems could give rise to complex cellular and tissue responses that determine the final functional outcome in vivo.

In this context, molecular mechanisms whereby CO and NO modulate the vascular tone in vivo have not completely been understood. In the liver, where endogenous NO production appears low,[2,11] CO is abundantly produced, and its cancellation by inhibiting the HO activity or capturing the gas directly causes sinusoidal constriction, indicating that the gas is necessary to maintain low vascular resistance in this organ.[2,3,15,16] In other organs producing relatively high NO, inhibitory effects of CO on the NO-mediated sGC activation have also been plausible; the transgenic mice with site-specific HO-1 overexpression in vascular smooth muscle cells (VSMCs) displayed systemic hypertension,[17] suggesting that HO-1–derived CO interferes with activation of sGC by endothelium-derived NO. Likewise, in the cerebral circulation, the effect of CO on vascular tone remains controversial.[18,19] The reason why the effect of CO in the very same organ varies among different studies has been unclear; however, the key to solve this inconsistency could lie in examining spatial relationship or anatomical proximity between gas-producing sites and their reception sites in the tissue that has been left from careful examination.

This study thus aimed to determine effects of suppressing endogenous CO derived from HO on local NO production and to relate those with changes in arteriolar tone. In addition to conventional immunohistochemical approaches, spatiotemporal information of local NO generation in the presence or absence of the CO suppression was collected in vivo directly with laser-confocal intravital microscopy. The results suggest that distinct from its action in the liver, CO is a tonic regulator against NO-dependent vasodilatation in the cerebral microcirculation of the adult rat.

Materials and Methods

General and Cranial Window Preparations

The procedures described in this article have been performed with the approval of the Animal Care and Use Committee of Keio University School of Medicine. Experiments were performed on male Wistar rats (280 to 350 g; CLEA Japan; Tokyo, Japan) that were not fasting before experiments. Rats were anesthetized with an intraperitoneal injection of α-chloralose (60 mg/kg) and urethane (600 mg/kg), tracheostomized, and spontaneously ventilated. The femoral artery and vein were cannulated for monitoring mean arterial pressure (MAP) and sampling arterial blood for the blood gas analysis. Rectal and window temperature were monitored and kept at 36°C to 37°C with the use of a thermostatically controlled heating lamp. The head of each rat was fixed in a stereotaxic frame, and the left parietal bone was exposed by a longitudinal midline skin incision. After three polyethylene tubes (PE-50; ID, 0.58 mm; OD, 0.965 mm) were fixed on the skull with cyanoacrylate, a closed cranial window was made with the use of a cover glass and quick self-curing acrylic resin (GC Unifast). The pial surface was then superfused with artificial cerebrospinal fluid (CSF); its composition was (mmol/L): 147.8 Na^+, 3.0 K^+, 2.3 Ca^{2+}, 135.2 Cl^-, 19.6 HCO_3^-, 1.67 lactate, 1.1 phosphate, and 3.9 glucose, equilibrated with 5% CO_2 and 5% O_2 balanced with N_2 at 37°C. The MAP, arterial CO_2 partial pressure (P_{CO2}), and arterial blood pH were kept within the normal range during experiments (Table).

Arterial Blood Pressure, Gases, and pH

	n	MAP (mm Hg)	pH	P_{CO2} (mm Hg)	P_{O2} (mm Hg)
Pre-experiment	25	109±2	7.41±0.03	32±4	86±14
Post-experiment	25	105±2	7.41±0.05	31±3	89±15

Values are mean±SD.

Immunohistochemical Analysis

Anesthetized rats were transcardially perfused with PBS for 5 minutes to remove blood. The specimens were fixed in paraformaldehyde-lysine-periodate solution at 4°C for 4 hours, cryoprotected, and embedded in optimal cutting temperature compound (Miles Laboratories). Coronal sections with 8-μm thickness were prepared at −20°C and incubated with optimal concentrations of antibodies. GTS-1 and GTS-2 are monoclonal antibodies (mAbs) raised against rat HO-1 and HO-2, respectively in our laboratory.[15] We also applied mAb 24G, which recognizes bilirubin (BR)–IXα[20]; because BR-IXα is generated from biliverdin-IXα, a regiospecific product of HO reactions, 24G7-specific immunoreactivities serve as a marker of HO-mediated degradation of heme and CO generation in vivo. Semiserial sections were also stained with mAbs against NOS1 and NOS3 (Transduction Laboratories), sGC (Wako Chemicals), and syntaxin (Sigma). These primary antibodies were detected by streptavidin/horseradish peroxidase–coupled secondary antibody (Vectastain Elite ABC kit; Vector Laboratories, Inc) and diaminobenzidine as a chromogen.

Determinations of Isozyme-Specific HO Activities and BR-IXα Content

HO activities were determined by measuring formation of BR-IXα as described previously.[21] To determine the HO-1–specific activity, we used GTS-3, an anti-rat HO-1 mAb, prepared in our laboratory. Microsomal fractions were prepared, and 50 μL of the microsomal samples were incubated with the same volume of either PBS or GTS-3 (0.5 mg/mL). When GTS-3 was added to the reaction mixture, it blocks the HO-1–specific enzyme activity with relatively low dose.[22] Total HO activity was determined by measuring BR-IXα production in the presence and absence of GTS-3.

BR-IXα content in CSF and effluents collected from superfusate were determined by an ELISA using mAb 24G7.[23]

Direct Detection of NO Production in the Pial Microcirculation

The pial microcirculation was observed through a cranial window with an upright microscope (Olympus BX51W1) using either a 20× (XLUMPlanFl, NA; 0.95) or a 40× (LUMPlanFl, NA; 0.8) water immersion lens. The microscopy was equipped with a silicon-intensified target camera (C2400–08; Hamamatsu Photonics) and a real-time laser-confocal imaging system (CSU21 confocal scanner; Yokogawa, Inc.) assisted by an 8-bit digital processor. Values for gain and offset of the camera as well as those for the laser-power supply were constant throughout the experiments.

To visualize NO-producing sites in vivo, diaminofluorescein-2 diacetate (DAF-2DA; Daiichi Pure Chemicals Co Ltd), an NO-sensitive fluoroprobe,[24,25] was superfused on the pial surface. The 60-minute superfusion of DAF-2DA (10 μmol/L) caused no significant elevation of adherent venular leukocytes. To collect microfluorographs of the NO-associated fluorescence, the pial surface was epi-illuminated by an excitation wavelength of 488 nm with a short exposure time <0.5 s at 20 and 60 minutes. The microscopic fields containing an unbranched segment of the arteriole (15 to 40 μm in diameter) were selected, and only those that shared the same focusing plane were examined.

To examine the spatial distribution of DAF-2 probe, we also used 4-aminofluorescein (4-AF) diacetate (Calbiochem), an NO-insensitive fluorophore. Because 4-AF cannot react with NO by forming a triazole-ring, its fluorescence intensity is insensitive to the

presence of NO; therefore, it has been used as a negative control for DAF-2. Fluorescence intensities of the two separate anatomical locations were quantified; at the arteriolar wall and at the extravascular cells located in the subarachnoid space. For the arteriolar wall, ≈400 measurements were taken as a single line-scan along the longitudinal axis of the vessel wall and 5 longitudinal line-scans with 0.4-μm steps between lines were taken and averaged. Therefore, a scanned area formed of ≈400×5 pixels represented 150×2 μm^2 in real space. For the extravascular cells, a size variable window (120×10 μm^2 in real space on average) was positioned at the area that shared the same focusing plane with the vessel walls.

Calibration of the fluorescence intensities was performed by determining gray levels of known concentrations of DAF-2 triazole (DAF-2T; Daiichi Pure Chemicals Co Ltd), a stable compound yielded by the interaction between DAF-2 and NO^+. The collected images were processed by the digital imaging software (MetaMorph 6.1; Universal Imaging Corporation), and the pixel-based data in the area of interest were converted into gray levels. Based on the calibration line, gray levels were converted into the corresponding concentrations of DAF-2T, designated as apparent DAF-2T concentrations ($DAF\text{-}2T_{app}$) at 20 minutes and 60 minutes. As an index of local NO production, the rate of elevation of $DAF\text{-}2T_{app}$ during this 40-minute (DAF-NO formation) was calculated using the following formula: DAF-NO formation $(nmol \cdot L^{-1} \cdot min^{-1}) = ([DAF\text{-}2T]_{app\ at\ 60\ minutes} - [DAF\text{-}2T]_{app\ at\ 20\ minutes})/40$ minutes.

NO Measurements in Cultured Porcine Aortic Endothelial Cells

Porcine aortic endothelial cells (PAECs) were harvested and cultured on type I collagen-coated dish in M199 medium supplemented with 10% FBS as reported.[26] NO production in cultured PAECs between passages 6 and 10 was assessed using the DAF-2DA as described previously.[25] Briefly, PAECs at 95% confluence were serum-depleted for 2 hours in DMEM containing HEPES (22 mmol/L). Cells were incubated with DAF-2DA (10 μmol/L) at 37°C for 20 minutes as the basal dye loading, and followed by 30-minute dye loading for measurements of DAF-NO formation. The NO formation was determined by calculating fractional changes in fluorescence intensities measured at 50 minutes versus those measured at 20 minutes. The fractional changes in the NO formation were expressed as values versus the controls, which were treated with the vehicle-containing medium. To examine actions of CO on the endothelial NO generation, tricarbonyldichlororuthenium (II) dimer (100 μmol/L; Sigma), a CO-releasing molecule (CORM), was added at 30 minutes before the basal dye loading. To test whether the effect of CO resulted from its specific binding to heme proteins, cells in the dishes were exposed to white light, which was provided by a fiber light guide equipped with a metal halide lamp (PMH-160; 150 W; Mejiro Precision) that covers wavelengths between 400 and 800 nm.[27,28] The experimental rig and the imaging systems were the same as those used for the study in vivo. At least 20 to 30 individual cells per dish were analyzed, and more than three separate sets of experiments were conducted for each group. Distinct from other gases with the heme-binding ability such as O_2 and NO, CO can be dissociated from the prosthetic heme easily on light exposure.[27,28] This experiment thus allowed us to prove whether the effect of CO on the NO generation resulted from the specific gas binding to the heme proteins, including NOS.

Using the same PAECs after depleting serum for 24 hours, immunoblotting of NOS3 and its phosphorylated form were performed according to previous methods.[26] Briefly, 30 to 40 μg of total protein was diluted in Laemmli buffer containing 5% β-mercaptoethanol, denaturated 5 minutes at 95°C, separated by SDS-PAGE (10% gels), and transferred onto polyvinylidene difluoride membranes. Membranes were saturated in PBS with 0.05% Tween 20 and 3% nonfat milk for 1 hour. Blocked membrane was incubated with an antibody directed against phospho-NOS3 (Ser-1177, Cell Signaling Technology) or that against NOS3 (Transduction Laboratories) at a dilution of 1:1000 in the same buffer for overnight at 4°C. Membrane was rinsed with PBS with Tween 20 and incubated with the horseradish peroxidase–conjugated secondary antibody for 1 hour. Proteins were detected with an ECL reagent on an x-ray film. When necessary, cells were treated with CORM or $RuCl_3$ at desired concentrations for 1 hour. H_2O_2, a reagent known to elicit phosphorylation of NOS3, was added at 200 μmol/L for 1 hour as a positive control.[26]

Statistics

Values are expressed as means±SE unless mentioned. Significant differences between means were evaluated using ANOVA followed by Fisher's test for multiple comparisons. Differences indicating P values <0.05 were considered statistically significant.

Results

Cell-Specific Localization of Gaseous Monoxide-Generating Systems in the Rat Cerebrum

To determine the distribution of CO- and NO-generating systems in the cerebrum, immunohistochemical analysis was performed. Appreciable HO-2 immunoreactivities were found in subdural mesothelial cells, arachnoid trabecular cells, the arteriolar endothelium in the subarachnoid space, and neural cells in parenchyma (Figure 1A and 1F). Immunoreactivities for NOS3 (Figure 1D and 1H) were clearly demonstrated in the endothelium, whereas those of NOS1 (Figure 1C and 1G) appeared to be almost indistinguishable from those of HO-2, indicating that the sites of CO production coincide with those of NO production. Likewise, such colocalization of HO-2 and NOS1 was evident in the hippocampal neuron (Figure 1J through 1N). To confirm whether expressed HO-2 degrades protoheme-IX to produce CO and, if so, to identify sites of CO production, the tissue was stained for BR-IXα, an end product of HO-mediated heme degradation. Figure 2 illustrates cell-specific distribution of gas-producing and reception sites in the vicinity of an arteriole. Immunoreactivities of mAb 24G7 indicated that BR-IXα occurred in arteriolar endothelia, VSMCs, and arachnoid trabecular cells, indicating actual CO generation by HO in these cells. BR-IXα was also detected in the CSF (0.8±0.2 μmol/L; n=6) and became immeasurable by the replacement with artificial CSF for 60 minutes. These results suggest that local heme degradation and CO generation by HO occurred in and around pial microvascular systems. Collectively, the site of HO activity indicated by BR-IXα appeared to overlap not only with that of NOS3 but also in part with that of NOS1. It should be noted that the tissue did not exhibit any notable immunoreactivities of HO-1 (data not shown).

To determine the isozyme-specific HO activities, mAb GTS-3 was used to inhibit HO-1–dependent activities. When mAb GTS-3 was added to the reaction mixture of the brain samples, it did not cause any reduction in the total HO activity compared with the basal activity measured in the presence of IgG (Figure 2F). On the other hand, adding mAb GTS-3 to the spleen sample substantially reduced the HO activity by ≈75% (Figure 2G), consistent with our previous observation in the rat spleen showing the activity ratio between HO-1 and HO-2 is ≈3:1.[22] Therefore, it appears that HO-2 is a major source for the catalytic activity of the enzyme in the brain, and HO-1 plays little role, if any, at least under normal conditions. Together, these results suggest that

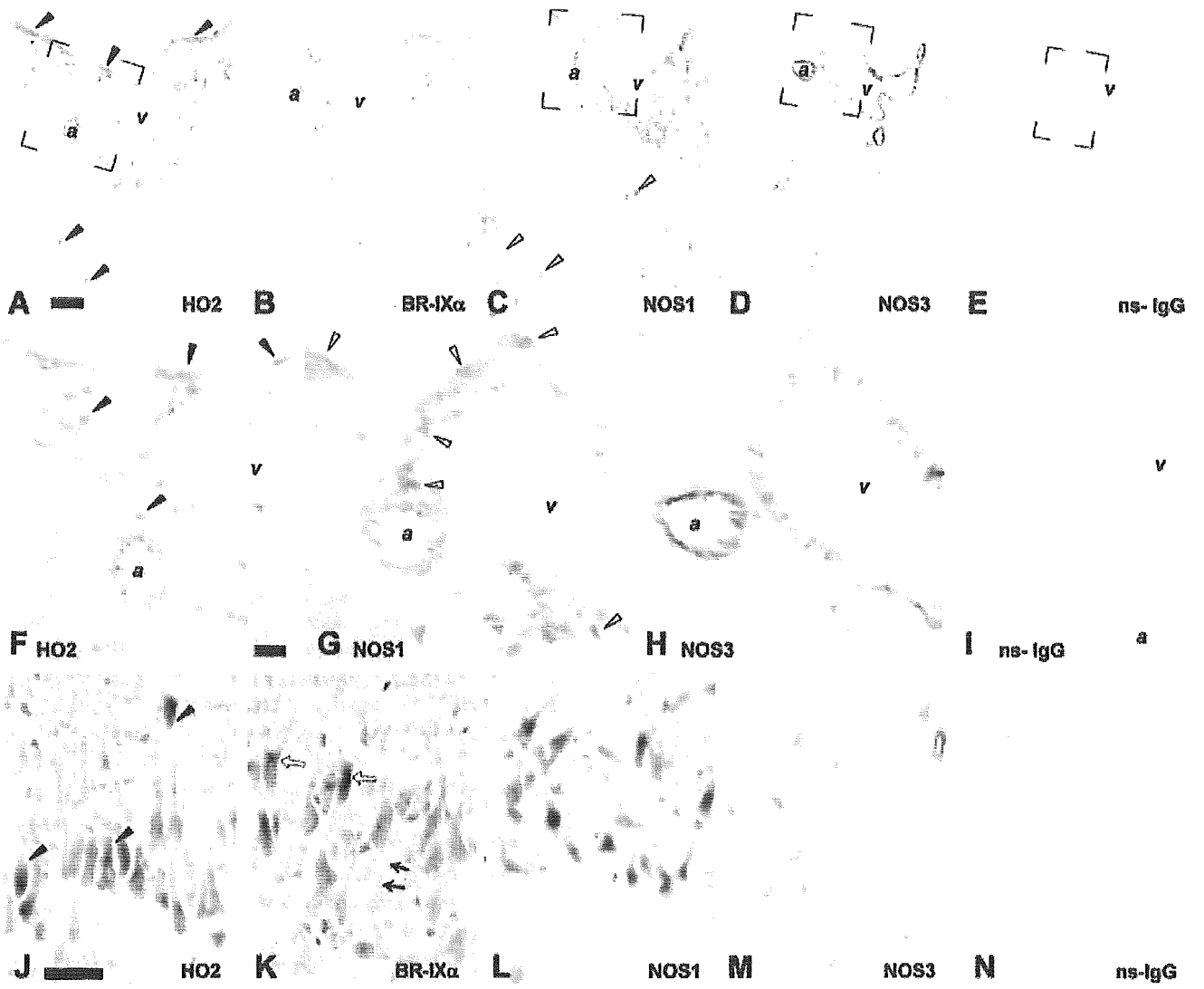

Figure 1. Distribution of CO- and NO-producing enzymes in the rat brain. A, Immunohistochemical staining for HO-2 in a coronal section of the cerebrum. Note strong labeling at subdural mesothelia and somata in the cortex (black arrowheads). B, Immunoreactivity for BR-IXα is weak but similar to those with HO-2. C, NOS1 immunoreactivity is similar to that of HO-2. Somata in the cortex show pronounced labeling of NOS1 (white arrowheads). D, NOS3 immunoreactivity is confined to the endothelium. Square marked by brackets in A, C, D, and E indicates the field shown in F, G, H, and I, with high magnification. F and G, Thin cells forming the subdural mesothelium and polygonal cells with round nuclei of the trabeculae exhibit strong labeling of HO-2 (black arrowheads) and of NOS1 (white arrowheads). H, Clear labeling of NOS3 is seen in the endothelium. J, Somata in the pyramidal layer of the hippocampus are HO-2 positive (black arrowheads). K, Some somata (white arrows) and processes of neurons (black arrows) are immunopositive for BR-IXα. L, Neurons demonstrate strong labeling for NOS1. M, Clear vascular labeling for NOS3. E, I, and N, Negative controls stained with nonspecific mouse IgG. Bars=50 μm in A and 30 μm in F and J. a indicates arteriole; v, venule.

pial arterioles reside in the environment where sources of CO and NO production are abundant. Interestingly, VSMCs of these vessels are juxtaposed luminally with endothelia and abluminally with arachnoid cells in which enzymatic sources of CO and NO colocalize.

Endogenous CO Suppression Elicits Vasodilatation of Cerebral Arterioles

To examine whether CO plays a role in regulating vascular tone, we attempted to inhibit endogenous CO production by zinc protoporphyrin IX (ZnPP), a competitive inhibitor of HO, and monitored changes in diameter of pial arterioles over a 60-minute period. Superfusion of ZnPP (0.01 to 1 μmol/L) caused a dose-dependent dilatation of pial arterioles. The ZnPP-induced dilatation occurred acutely, being noticeable at as early as 10 minutes after the start of its superfusion at 0.1 μmol/L. The highest dose (1.0 μmol/L) of the inhibitor induced a robust dilatation (54±5% at 60 minutes), whereas the same dose of copper protoporphyrin (CuPP), which does not block the HO activity, caused no significant changes (Figure 3A and 3B). Such dilatation elicited by the CO suppression was significantly reduced by supplementing CO (10 μmol/L) locally. Furthermore, this dilatation by the HO inhibition appears NO-dependent because N^{ω}-nitro-L-arginine methyl ester (L-NAME; 1 mmol/L) but not N^{ω}-D-nitroarginine methyl ester (D-NAME; 1 mmol/L), attenuated the response (Figure 3C). To note is that a CO-free vehicle superfusion caused a small but notable dilatation (5.9±3.6%

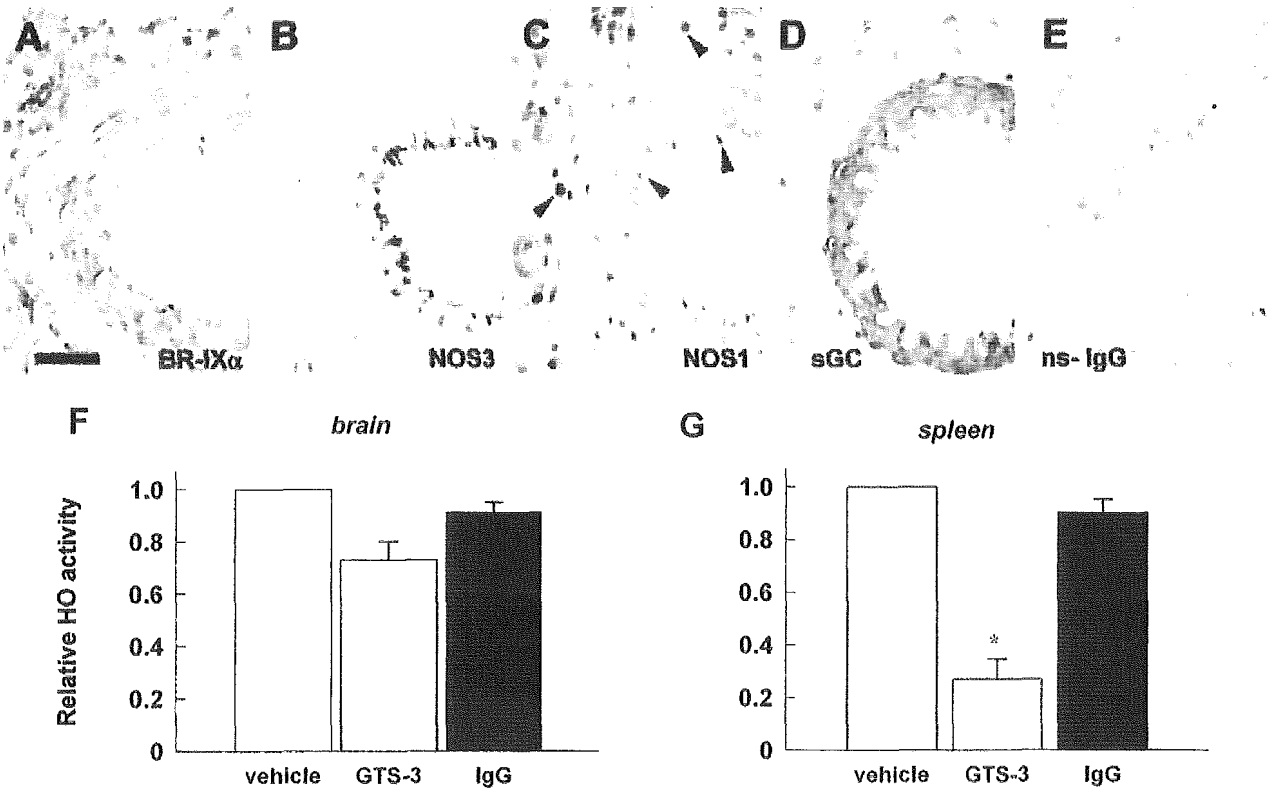

Figure 2. Cell-specific distribution of gas-producing and reception systems in the vicinity of an arteriole. A, BR-IXα immunoreactivities occur in different cells including endothelia, VSMCs, and arachnoid trabecular cells. Bar=30 μm. B, Endothelia exhibit concentrated labeling for NOS3. C, Part of endothelia and arachnoid trabecular cells demonstrate labeling for NOS1 (black arrows). D, sGC is expressed in VSMCs. E, A negative control stained with nonspecific mouse IgG. F and G, Isozyme-specific inhibition of HO activities using GTS-3, a mAb against rat HO-1. Note that GTS-3 suppresses the HO activities of the spleen samples but not of the brain samples. HO activities are expressed as relative values vs the vehicle-treated control. Data represent mean±SE of three separate measurements. *$P<0.05$ compared with the IgG control.

at 60 minutes), and the dilatation was abolished (−0.1±1.9% at 60 minutes) by the superfusion of exogenous CO (10 μmol/L). Such a dilatory event could be a result of eliminating CO in the CSF so far as judged from the local BR-IXα measurements and is consistent with a putative role of this gas acting as a tonic regulator on arteriolar tone.

Three-Dimensional Reconstitution and Quantitative Characterization of NO Generation In Vivo

Aforementioned results suggesting a role of CO in modulating the NO-mediated vasodilatation led us to examine changes in local NO generation quantitatively in and around pial arterioles. Having obtained heterogeneous distribution of gaseous monoxide-generating enzymes even within this thin layer of the arachnoid (Figure 1A through 1I), the assessment must be performed vertically as well as horizontally through the layer. To achieve this prerequisite, we used confocal diaminofluorescein microfluorography to determine spatial and temporal alterations of NO generation in real-time and constructed 3D mapping of the gas. Panel 1 of Figure 4A shows NO-associated fluorescence right below the surface of dura. When the focal plane was moved 20 μm more deeply (panel 2), the arteriolar wall and cells residing in the arachnoid space became more fluorescent. This observation appears to be consistent with the vertical distribution of NOS-positive cells, including endothelia, subdural mesothelial cells, and arachnoid trabecular cells (Figure 1G and 1H). Spatial relationship between panels 1 and 5 of Figure 4A could correspond to the focal planes indicated by the top and the bottom hairlines in Figure 4B. Microvessels residing in the superficial layer lying no more than 100 μm from the dura were subjected to this study. Our methodology allowed us to examine NO generation occurring in these sites. For a series of experiments described in later sections, attention was paid to obtain fluorography focused at the center of the vessel, namely at the point where the largest diameter was seen. By so doing, we could avoid capturing saturated fluorescence that was typically derived from subdural mesothelial cells.

We conducted another control experiment to test whether a constant superfusion of DAF-2DA, an NO capturing reagent, affects vasodilatory response. To do this, we measured arteriolar diameter over a 60-minute period after blocking HO by ZnPP in the presence and absence of DAF-2DA. As seen in Figure 4C, the presence of DAF-2DA (10 μmol/L) significantly blunted vasodilatory response elicited by ZnPP, eliciting a >50% reduction, suggesting that presence of the fluoroprobe restricts the local amount of NO.

The central assumption in the measurement of NO is that a change in a fluorescence intensity represents a proportional change in the number of DAF-2T molecules present in recorded images. We tested this assumption by collecting

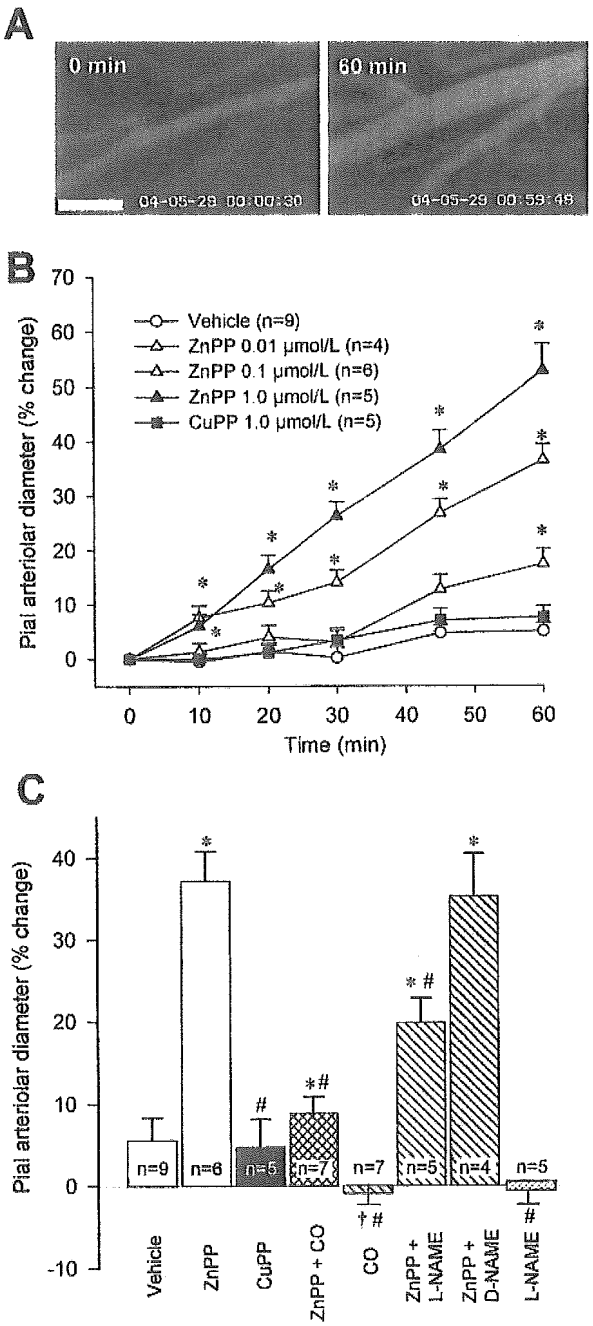

Figure 3. Changes in vasodilatory response on alterations in CO and NO generation. A, Typical changes in arteriolar diameter in response to ZnPP. Bar=100 μm. B, Time course of changes in arteriolar diameter in response to the superfusion of the HO inhibitor at different concentrations. C, Summary data of changes in arteriolar diameter at 60 minutes after the superfusion of various reagents. Supplementation of CO (10 μmol/L) significantly reduces the vasodilatory response induced by the HO inhibition. L-NAME (1 mmol/L) but not D-NAME (1 mmol/L) abolishes this vasodilatation. Diameters are standardized as a percentage of baseline diameters before applying the reagents. *$P<0.05$ an increase compared with the vehicle-treated control. †$P<0.05$ a decrease compared with the vehicle-treated control. #$P<0.05$ compared with the ZnPP-treated group. Values are mean±SE.

fluorescence images from a well filled with DAF-2T in CSF at pH 7.4. Intensities of NO-associated fluorescence were calibrated with known concentrations of DAF-2T. As seen in Figure 4D, the 8-bit gray levels measured through a digital processor were fitted to the second-order polynomial regression. The relationship obtained from three separate measurements was summarized by the following expression: gray level=34.0+0.068 [DAF-2T]+0.0012[DAF-2T]^2 (r^2=0.995).

Suppression of Endogenous CO Stimulates NO Generation and Vasodilatation

To explore the mechanism whereby CO tonically inhibits NO-mediated vasodilatation, we examined the effect of the HO inhibitor on endogenous NO generation using laser-scanning microfluorography. Figure 5A illustrates a series of representative images tracing time-dependent elevation of NO in the pial microcirculation. The first image in the series was taken at 20 minutes after the start of DAF-2DA superfusion; the time just as the vessel wall began to appear fluorescent. In subsequent images taken at 60 minutes, the intensity of fluorescence increased at vascular walls and the cells in extravascular space, suggesting continuous NO generation in these cells. When ZnPP, but not CuPP, was superfused, the DAF-2T fluorescence was already more intense at 20 minutes, and the extent of time-dependent elevation in the fluorescence appeared to be greater than that under the control condition, indicating accelerated production of NO under the CO-suppressed condition. Because not only NO amount but also the esterase activity might determine intensities of the fluorescence, we examined spatial distribution of intracellular esterase activities by loading 4-aminofluorescein diacetate (4AF-DA), an NO-insensitive probe of which the structure is similar to that of DAF-2DA. Unlike spatially heterogeneous elevation of DAF-2T fluorescence, with 4AF-DA, most of arachnoid trabecular cells and microvascular endothelium were stained homogeneously, displaying a pattern of the fluorescence distinct from that with DAF-2DA (Figure 5A, bottom). This observation led us to conclude that a temporal rise in DAF-2T fluorescence was attributed to NO generation, not to the esterase activity.

Figure 5B and 5C summarize quantitative analyses of changes in local NO production expressed as the rate of elevation of DAF-2T$_{app}$ per unit of time. At vascular walls, CO suppression by ZnPP in the tissue, but not by CuPP, caused a significant increase in NO generation approximately by 70%, suggesting that its stimulatory effect on the NO generation results from a specific inhibitory action on HO. Superfusion of CO together with ZnPP completely reversed this elevation to the basal level. To test further whether this effect of CO supplementation was attributable to an inhibitory action on NOS, we simultaneously administered the HO inhibitor with L-NAME. Such a concomitant inhibition of CO- and NO-producing enzymes attenuated the enhanced NO production. When the cells in the extravascular space were examined, altered patterns of changes in NO production were similar to those measured at the vascular walls. However, one distinct point was that CO superfusion caused a more pronounced reduction in NO generation at the extravascular cells than at the vascular walls (45% versus 20%). It may conform to the existence of NO source, which is independent of NOS in circulation.[29] Collectively, these results suggest that CO derived from HO interferes with the NO production.

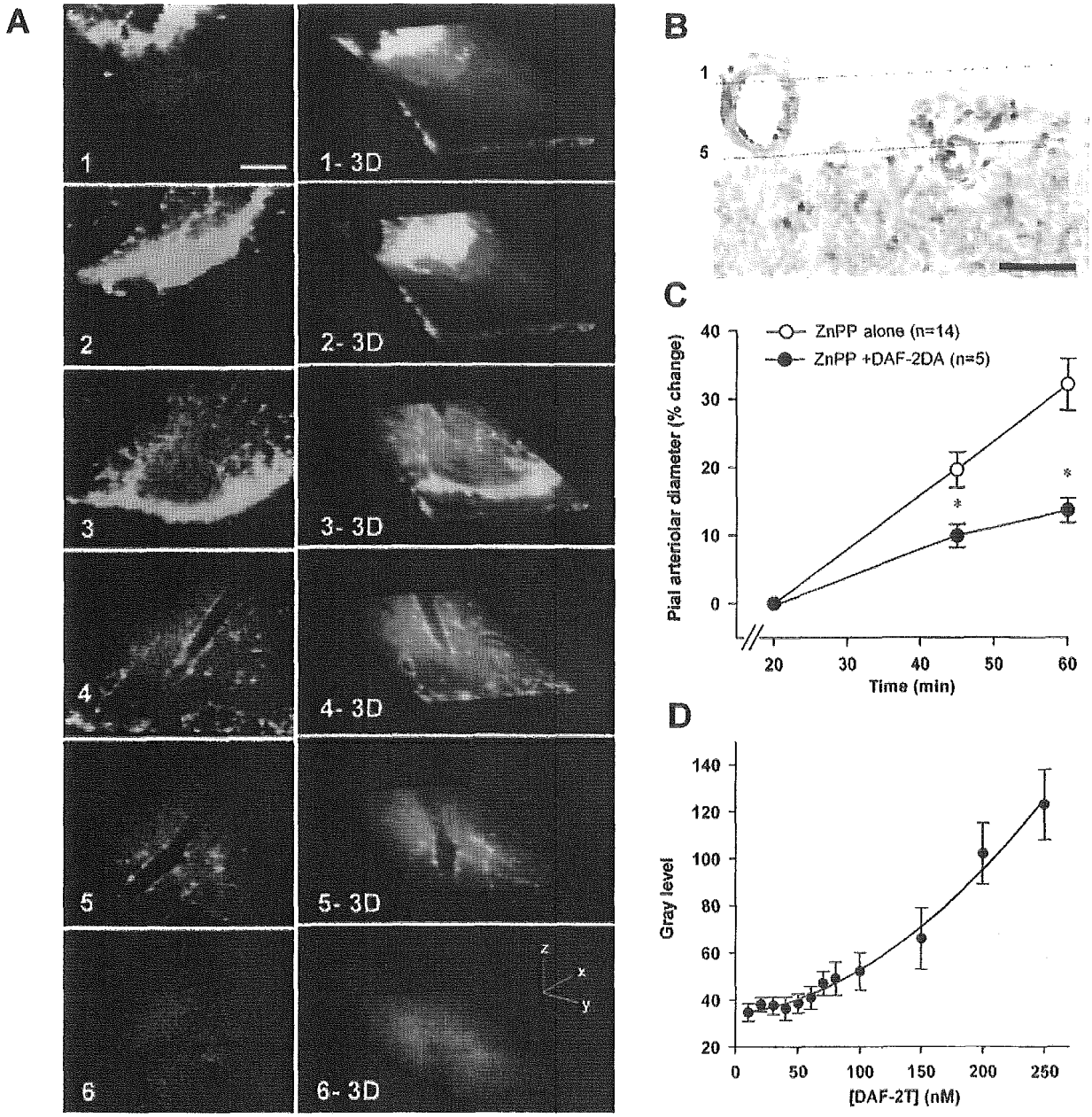

Figure 4. Three-dimensional reconstitution and quantitative characterization of NO generation at the surface of rat cerebrum. A, Two-dimensional images of NO-associated fluorescence at 60 minutes after the start of the DAF-2DA superfusion. At each *x-y* confocal plane, a 2D image is obtained and these images are stacked in sequential order with an imaging software to yield 3D images of the rat cerebral surface. Representative images of six different *x-y* planes covered 150-μm depth of the tissue, and images are either 20 or 30 μm apart. Note that the surface of arachnoid membrane, the cells in subarachnoid space, and the wall of blood vessels exhibit NO-associated fluorescence. Bar=100 μm. B, The section transversing *x-z* plane is incubated with an mAb against syntaxin, an integral protein abundantly expressed in neurons. Arachnoid membrane composed of subdural mesothelial cells and trabecular cells, and the blood vessels are devoid of syntaxin-positive staining, and these cells appear to represent the origin of the fluorescence seen in A. Two parallel lines indicated here could correspond to the spatial relationship between panels 1 and 5 of A. Bar=100 μm. C, The effect of a constant superfusion of DAF-2DA on vasodilatory response induced by the HO inhibition. *$P<0.05$ compared with the group superfused with ZnPP alone. D, The relationship between concentrations of DAF-2T and gray level of the fluorescence intensities is determined in vitro (n=3).

CO Suppresses NO Generation in Cultured Endothelial Cells

To examine mechanisms for CO to antagonize endothelial NO generation, we set out experiments in vitro using PAECs. Likewise to observations in vivo, PAECs displayed a notable NO generation as judged by an increase in DAF-2T fluorescence (Figure 6A, top row). Preincubation with CORM (100 μmol/L) significantly suppressed the NO generation (Figure 6A, middle row; and 6B). The CO-induced changes were cancelled by exposing these cells to white light, whereas the light exposure per se did not alter the basal NO generation. Suppression of the NO generation by CO was unlikely to occur through downregulation of NOS3 expression or that of the enzyme phosphorylation, as judged by immunoblotting

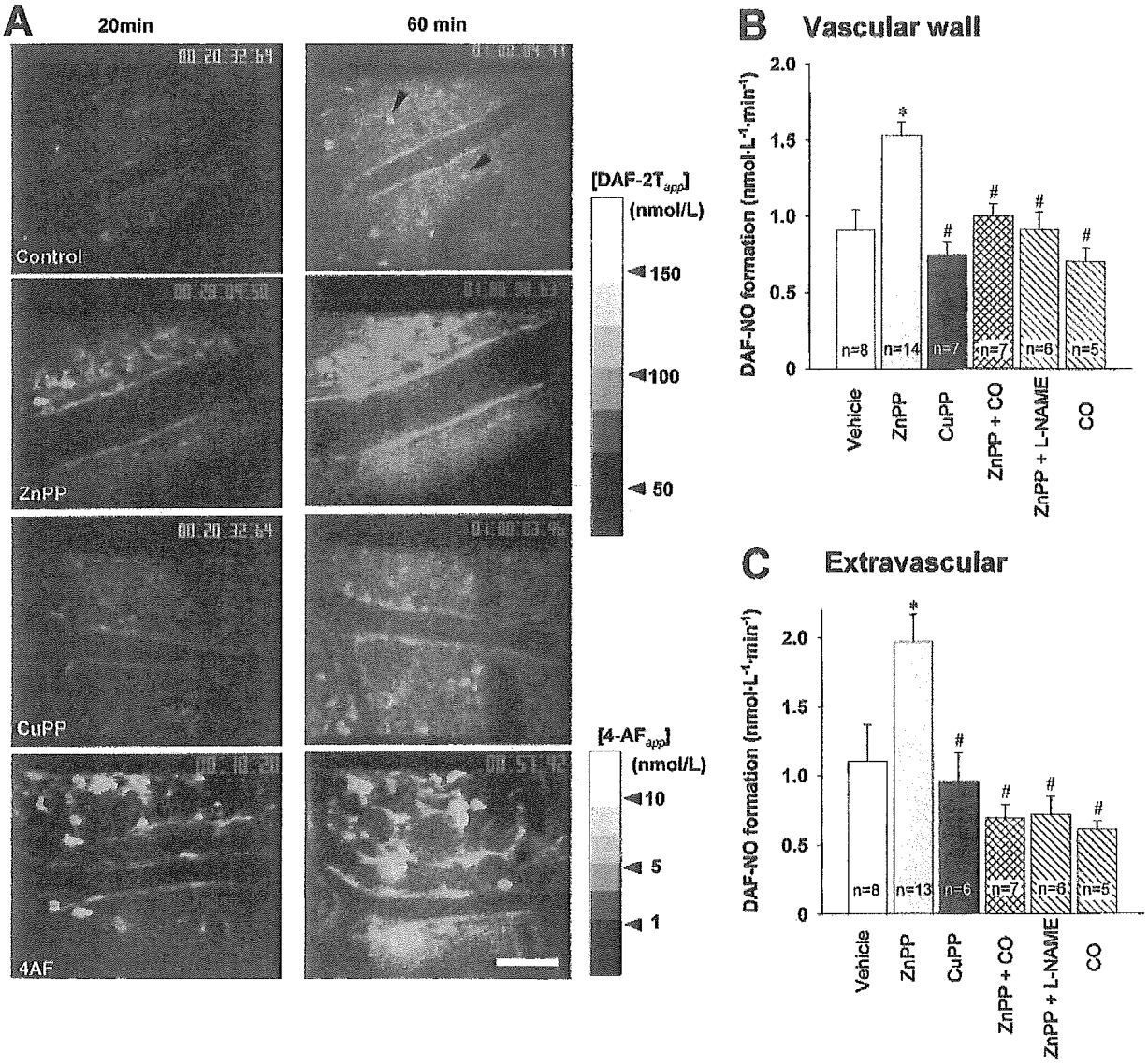

Figure 5. Augmented NO generation under CO-suppressed conditions. A, Time-dependent elevation of NO production in the pial microcirculation. In the control- and the CuPP-treated groups, NO-associated fluorescence is faint at 20 minutes; it then becomes obvious at the vascular walls and at the cells located in extravascular space (arrowheads) at 60 minutes. On the other hand, in ZnPP-treated group, evident fluorescence is exhibited even at 20 minutes, and it increases further at 60 minutes. 4AF-DA, an NO-insensitive fluorescence precursor, is used as a control. B, Quantitative analyses of NO generation at the arteriolar walls. Local gray level intensities measured in vivo are converted to apparent concentrations of DAF-2T (DAF-2T$_{app}$) on the basis of calibration shown in Figure 4D. As an index of local NO formation, rate of elevation of DAF-2T$_{app}$ during this 40-minute (DAF-NO formation) is calculated (see Methods). C, The analyses for the cells located in the extravascular space. *P<0.05 and #P<0.05 compared with the vehicle-treated control and the ZnPP-treated groups, respectively. Values are mean±SE.

using the specific antibodies (Figure 6C). These results suggest that the ability of CO to bind to the prosthetic heme plays an important role in inhibiting endothelial NO generation.

Discussion

Our findings provide evidence that CO produced by constitutive HO can attenuate vasodilatory responses of arterioles by interfering with NO generation in the rat brain. In this study, the physiologic relevance of CO production in cerebral microcirculation is supported by the results of two independent experimental approaches: measurements of pial arteriolar diameter under conditions in which endogenous CO or NO production was varied, and direct detection of NO in situ using the fluoroprobe under normal and CO-suppressed conditions. The use of confocal microscopy together with the immunohistochemical detection of gas-producing enzymes allowed us to obtain spatial and temporal information of CO-modulated NO production in cerebral microcirculation.

There are several mechanisms whereby the HO-CO system modulates NO-dependent biological events. First, inhibition of the HO activity could allow NOS to use intracellular NADPH and O_2 less competitively, thereby causing increased NOS activities. Because NADPH is an intracellular substance that cannot be transported across the cell, HO and NOS are required to reside in the same cell for such a competition to

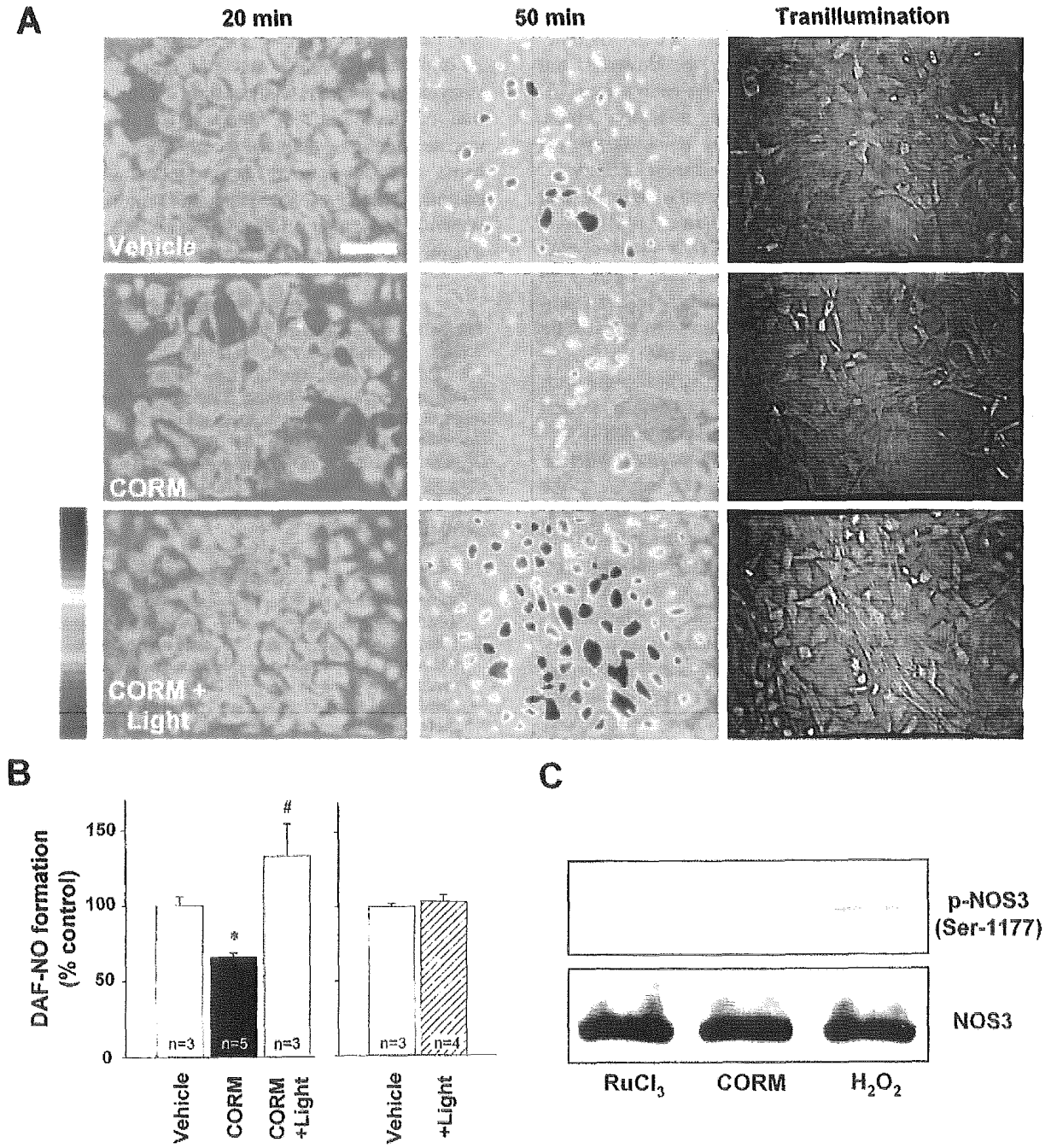

Figure 6. Effects of CORM on NO generation and NOS3 phosphorylation in PAECs. A, Representative fluorescent images of PAECs loaded with DAF-2DA. Left and middle columns, pseudocolor representation of micrographs captured at 20 minutes and 50 minutes after loading of DAF-2DA (10 μmol/L), respectively. Right column, transillumination micrographs after each experiment. Treatment with CORM (middle row) attenuates the basal DAF-NO formation (top row), and this attenuation is cancelled by exposure to white light in the presence of CORM (bottom row). Bar=100 μm. A color bar showing blue, green, yellow, and red indicates the increasing fluorescence intensities. B, Fractional changes in fluorescence intensities indicative of NO production. Data were collected from ≈20 to 30 individual cells from each experiment. Values are mean±SE from 3 to 5 separate experiments. *$P<0.05$ and #$P<0.05$ compared with the vehicle-treated control and the CORM-treated groups, respectively. C, Effects of CORM on expression of NOS3 and phospho-NOS3. PAECs were treated with $RuCl_3$ (100 μmol/L), CORM (100 μmol/L), or H_2O_2 (200 μmol/L), a reagent eliciting the enzyme phosphorylation, for 1 hour. Cell proteins were obtained and eNOS expression and phosphorylation of eNOS at Ser1179 were determined with the immunoblotting. Representative for 4 independent experiments.

take place. Second, oxidative degradation of heme by HO could downregulate catalytic activities of heme enzymes including NOS.[30] Third, the ability that CO binds to ferrous heme of NOS raises a possibility that the gas directly inhibits the enzyme. Although this mechanism is supported by the previous study using purified NOS,[9] it remains unknown whether CO can suppress the NOS activity directly in the endothelial cells. Our current results indicating the acute photo-reversible action of CO on the endothelial NO generation in culture (Figure 6A and 6B) make this possibility

likely. It remains still unknown, through the same mechanism, whether CO generated in the cerebrovascular endothelium could inhibit NO generation in vivo. However, our observation showing an acute action of the endogenous CO suppression on the NO-mediated arteriolar dilatation (Figure 3B) supports the concept that the gas could target the prosthetic heme of NOS3 to inhibit the catalytic activity.

Our immunohistochemical analyses clearly indicate that HO-2 colocalizes with NOS isozymes (Figures 1 and 2). It is this colocalization that enables one gas, CO, to interfere with the formation of another gas, NO, and consequently to antagonize its vasodilatory response. Without such an anatomical arrangement, CO may not be able to change cellular responses mediated by NO. An inhibitory effect of CO on local NO production should be compared with our previous study using transgenic mice that exhibit systemic hypertension through cell-specific HO-1 overexpression in VSMCs.[17] In this case, it is sGC, but not NOS, that colocalizes with the CO-producing enzyme. With this, CO can suppress the activity of sGC in the same VSMC, and by so doing, antagonize NO-mediated vasodilatation. To note is the failure of CO to inhibit NO formation occurring in the neighboring endothelia, minimizing a possibility for CO to exhibit its paracrine effect. This reinforces further the significance of anatomical proximity and leads us to reconsider an ordinary concept that gases freely diffuse through plasma membrane. Indeed, it has been proposed that erythrocyte membrane retards transport of gases such as NO[31] and O_2[32] into the cell by forming a significant diffusion barrier. Such a possibility for CO should be examined further.

Collectively with our previous studies,[2,11,15] CO can regulate vascular tone at least by three distinct ways that depend on microanatomical arrangements of generation and reception of the vasoactive gases. First in the liver, CO modestly stimulates sGC in hepatic stellate cells, thereby reducing the tonic contractile tension of sinusoids where local amount of NO is low.[2,11,33] Second, in resistance arterioles, where there are sufficient amounts of NO, CO could target sGC to interfere with NO-mediated vasodilatation. Previous observation that transgenic mice exhibit systemic hypertension through cell-specific HO-1 overexpression in VSMCs[17] falls into this category. Third, in the cerebral microcirculation, CO interferes with NOS activities as a first step and subsequently reduces NO generation, thereby limiting vasodilatation. Which route, the second or the third, the gas takes to exert its action depends on which enzyme system, either sGC or NOS, HO colocalizes with. Such a notion could explain the complexity of vasoactive actions of CO, which have been reported in experimental models similar to our study: in newborn pigs, either CO or heme-L-lysinate, an exogenous HO substrate, dilates cerebral arterioles,[19] whereas inhibition of HO by chromium mesoporphyrin caused vasodilatation in the same system.[19] Further evaluation of anatomical proximity among the gas-producing enzymes and their reception systems should clarify mechanisms behind these observations.

In conclusion, the current study enables us to unravel physiologic roles of CO or constitutive HO on the regulation of neural and vascular functions in the brain. In view of a recent proposal that HO-2 is an oxygen sensor reducing CO generation in response to a decrease in local O_2 tension,[34,35] an implication could be made on a possible role of the HO isozyme on hypoxia-induced and NO-mediated vasodilatation in the brain.[36–38] Because CO in and around pial microcirculation could be overproduced by an increase in heme as a substrate or by an induction of HO-1 under conditions such as subarachnoid hemorrhage[39] and focal ischemia,[40] aberrant actions of this gas under these pathologic circumstances deserve further investigation.

Acknowledgments

This work was supported by Japan Society for the Promotion of Science, Grant-In-Aid for Scientific Research, 15500267 and 17500261 (to M.K.), Health Labor Sciences Research Grant, Research on Advanced Medical Technology from the Ministry of Health Labor and Welfare, and Grant-in-Aid for Creative Scientific Research, Leading Project for Biosimulation, the 21st Century Center-of-Excellence Program from the Ministry of Education, Culture, Sports, Science and Technology in Japan (to M.S.). We thank Ritsuko Hoshino, Rei Hasegawa, and Kyoko Ishiwata for technical assistance.

References

1. Verma A, Hirsch DJ, Glatt CE, Ronnett GV, Snyder SH. Carbon monoxide: a putative neural messenger. *Science.* 1993;259:381–384.
2. Suematsu M, Goda N, Sano T, Kashiwagi S, Egawa T, Shinoda Y, Ishimura Y. Carbon monoxide: an endogenous modulator of sinusoidal tone in the perfused rat liver. *J Clin Invest.* 1995;96:2431–2437.
3. Suematsu M, Kashiwagi S, Sano T, Goda N, Shinoda Y, Ishimura Y. Carbon monoxide as an endogenous modulator of hepatic vascular perfusion. *Biochem Biophys Res Commun.* 1994;205:1333–1337.
4. Moncada S, Palmer RM, Higgs EA. Nitric oxide: physiology, pathophysiology, and pharmacology. *Pharmacol Rev.* 1991;43:109–142.
5. Ryter SW, Morse D, Choi AM Carbon monoxide: to boldly go where NO has gone before. *Sci STKE.* 2004;2004:RE6.
6. Maines MD. Heme oxygenase: function, multiplicity, regulatory mechanisms, and clinical applications. *FASEB J.* 1988;2:2557–2568.
7. Taille C, El-Benna J, Lanone S, Dang MC, Ogier-Denis E, Aubier M, Boczkowski J. Induction of heme oxygenase-1 inhibits NAD(P)H oxidase activity by down-regulating cytochrome b558 expression via the reduction of heme availability. *J Biol Chem.* 2004;279:28681–28688.
8. Wang J, Lu S, Moenne-Loccoz P, Ortiz de Montellano PR. Interaction of nitric oxide with human heme oxygenase-1. *J Biol Chem.* 2003;278:2341–2347.
9. White KA, Marletta MA. Nitric oxide synthase is a cytochrome P-450 type hemoprotein. *Biochemistry.* 1992;31:6627–6631.
10. Scheele JS, Kharitonov VG, Martasek P, Roman LJ, Sharma VS, Masters BS, Magde D. Kinetics of CO ligation with nitric-oxide synthase by flash photolysis and stopped-flow spectrophotometry. *J Biol Chem.* 1997;272:12523–12528.
11. Suematsu M, Ishimura Y. The heme oxygenase-carbon monoxide system: a regulator of hepatobiliary function. *Hepatology.* 2000;31:3–6.
12. Kajimura M, Shimoyama M, Tsuyama S, Suzuki T, Kozaki S, Takenaka S, Tsubota K, Oguchi Y, Suematsu M. Visualization of gaseous monoxide reception by soluble guanylate cyclase in the rat retina. *FASEB J.* 2003;17:506–508.
13. Koesling D, Friebe A. Soluble guanylyl cyclase: structure and regulation. *Rev Physiol Biochem Pharmacol.* 1999;135:41–65.
14. Kajimura M, Goda N, Suematsu M. Organ design for generation and reception of CO: lessons from the liver. *Antioxid Redox Signal.* 2002;4:633–637.
15. Goda N, Suzuki K, Naito M, Takeoka S, Tsuchida E, Ishimura Y, Tamatani T, Suematsu M. Distribution of heme oxygenase isoforms in rat liver. Topographic basis for carbon monoxide-mediated microvascular relaxation. *J Clin Invest.* 1998;101:604–612.
16. Kyokane T, Norimizu S, Taniai H, Yamaguchi T, Takeoka S, Tsuchida E, Naito M, Nimura Y, Ishimura Y, Suematsu M. Carbon monoxide from heme catabolism protects against hepatobiliary dysfunction in endotoxin-treated rat liver. *Gastroenterology.* 2001;120:1227–1240.

17. Imai T, Morita T, Shindo T, Nagai R, Yazaki Y, Kurihara H, Suematsu M, Katayama S. Vascular smooth muscle cell-directed overexpression of heme oxygenase-1 elevates blood pressure through attenuation of nitric oxide-induced vasodilation in mice. *Circ Res.* 2001;89:55–62.
18. Brian JE Jr, Heistad DD, Faraci FM. Effect of carbon monoxide on rabbit cerebral arteries. *Stroke.* 1994;25:639–643.
19. Leffler CW, Nasjletti A, Yu C, Johnson RA, Fedinec AL, Walker N. Carbon monoxide and cerebral microvascular tone in newborn pigs. *Am J Physiol Heart Circ Physiol.* 1999;276:H1641–H1646.
20. Yamaguchi T, Wakabayashi Y, Tanaka M, Sano T, Ishikawa H, Nakajima H, Suematsu M, Ishimura Y. Taurocholate induces directional excretion of bilirubin into bile in perfused rat liver. *Am J Physiol.* 1996;270: G1028–G1032.
21. Ozawa N, Goda N, Makino N, Yamaguchi T, Yoshimura Y, Suematsu M. Leydig cell-derived heme oxygenase-1 regulates apoptosis of premeiotic germ cells in response to stress. *J Clin Invest.* 2002;109:457–467.
22. Makino N, Suematsu M, Sugiura Y, Morikawa H, Shiomi S, Goda N, Sano T, Nimura Y, Sugimachi K, Ishimura Y. Altered expression of heme oxygenase-1 in the livers of patients with portal hypertensive diseases. *Hepatology.* 2001;33:32–42.
23. Izumi Y, Yamazaki M, Shimizu S, Shimizu K, Yamaguchi T, Nakajima H. Anti-bilirubin monoclonal antibody. II. Enzyme-linked immunosorbent assay for bilirubin fractions by combination of two monoclonal antibodies. *Biochim Biophys Acta.* 1988;967:261–266.
24. Kashiwagi S, Kajimura M, Yoshimura Y, Suematsu M. Nonendothelial source of nitric oxide in arterioles but not in venules: alternative source revealed in vivo by diaminofluorescein microfluorography. *Circ Res.* 2002;91:e55–e64.
25. Kojima H, Nakatsubo N, Kikuchi K, Kawahara S, Kirino Y, Nagoshi H, Hirata Y, Nagano T. Detection and imaging of nitric oxide with novel fluorescent indicators: diaminofluoresceins. *Anal Chem.* 1998;70: 2446–2453.
26. Thomas SR, Chen K, Keaney JF, Jr. Hydrogen peroxide activates endothelial nitric-oxide synthase through coordinated phosphorylation and dephosphorylation via a phosphoinositide 3-kinase-dependent signaling pathway. *J Biol Chem.* 2002;277:6017–6024.
27. Wilson DF, Mokashi A, Chugh D, Vinogradov S, Osanai S, Lahiri S. The primary oxygen sensor of the cat carotid body is cytochrome a3 of the mitochondrial respiratory chain. *FEBS Lett.* 1994;351:370–374.
28. Antonini E, Brunori M. North-Holland Reserch Monographs: Frontiers of Biology. In: Neuberger A, Tatum EL, eds. *The Derivatives of Ferrous Hemoglobin and Myoglobin: Hemoglobin and Myoglobin in Their Reactions With Ligands.* Amsterdam, the Netherlands: North-Holland Publishing Company; 1971:13–39.
29. Stamler JS, Jia L, Eu JP, McMahon TJ, Demchenko IT, Bonaventura J, Gernert K, Piantadosi CA. Blood flow regulation by S-nitrosohemoglobin in the physiological oxygen gradient. *Science.* 1997;276:2034–2037.
30. Haider A, Olszanecki R, Gryglewski R, Schwartzman ML, Lianos E, Kappas A, Nasjletti A, Abraham NG. Regulation of cyclooxygenase by the heme-heme oxygenase system in microvessel endothelial cells. *J Pharmacol Exp Ther.* 2002;300:188–194.
31. Huang KT, Han TH, Hyduke DR, Vaughn MW, Van Herle H, Hein TW, Zhang C, Kuo L, Liao JC. Modulation of nitric oxide bioavailability by erythrocytes. *Proc Natl Acad Sci U S A.* 2001;98:11771–11776.
32. Coin JT, Olson JS. The rate of oxygen uptake by human red blood cells. *J Biol Chem.* 1979;254:1178–1190.
33. Bautista AP, Spitzer JJ. Inhibition of nitric oxide formation in vivo enhances superoxide release by the perfused liver. *Am J Physiol.* 1994; 266:G783–G788.
34. Prabhakar NR, Dinerman JL, Agani FH, Snyder SH. Carbon monoxide: a role in carotid body chemoreception. *Proc Natl Acad Sci U S A.* 1995; 92:1994–1997.
35. Williams SE, Wootton P, Mason HS, Bould J, Iles DE, Riccardi D, Peers C, Kemp PJ. Hemoxygenase-2 is an oxygen sensor for a calcium-sensitive potassium channel. *Science.* 2004;306:2093–2097.
36. Faraci FM, Heistad DD. Regulation of the cerebral circulation: role of endothelium and potassium channels. *Physiol Rev.* 1998;78:53–97.
37. Coney AM, Marshall JM. Role of adenosine and its receptors in the vasodilatation induced in the cerebral cortex of the rat by systemic hypoxia. *J Physiol (Lond).* 1998;509:507–518.
38. Pelligrino DA, Wang Q, Koenig HM, Albrecht RF. Role of nitric oxide, adenosine, *N*-methyl-D-aspartate receptors, and neuronal activation in hypoxia-induced pial arteriolar dilation in rats. *Brain Res.* 1995;704: 61–70.
39. Suzuki H, Kanamaru K, Tsunoda H, Inada H, Kuroki M, Sun H, Waga S, Tanaka T. Heme oxygenase-1 gene induction as an intrinsic regulation against delayed cerebral vasospasm in rats. *J Clin Invest.* 1999;104: 59–66.
40. Bergeron M, Ferriero DM, Vreman HJ, Stevenson DK, Sharp FR. Hypoxia-ischemia, but not hypoxia alone, induces the expression of heme oxygenase-1 (HSP32) in newborn rat brain. *J Cereb Blood Flow Metab.* 1997;17:647–658.